Science of the Total Environment 918 (2024) 170703

Contents lists available at ScienceDirect

Science of the Total Environment

journal homepage: www.elsevier.com/locate/scitotenv

An algorithm to generate 2D bathymetry of an Alpine river for habitat suitability assessment.

L. Stucchi [a], D. Fugazza [b,*], A. Sharifi [a], G. Traversa [c], G. Diolaiuti [b], D. Bocchiola [a]

[a] Department of Civil and Environmental Engineering, Politecnico di Milano, Milan, Italy
[b] Department of Environmental Science and Policy, University of Milan, Milan, Italy.
[c] Institute of Polar Sciences, National Research Council of Italy, 20125 Milan, Italy

HIGHLIGHTS

- A new methodology to generate 2D riverbed is presented.
- Point cloud bathymetry is used to model riffle-pool sequence.
- Drone data are used to recreate riverbed in ungauged area.
- Perlin noise is included to mimic the riverbed irregularities.
- Habitat Suitability is studied basing on generated river topography.

GRAPHICAL ABSTRACT

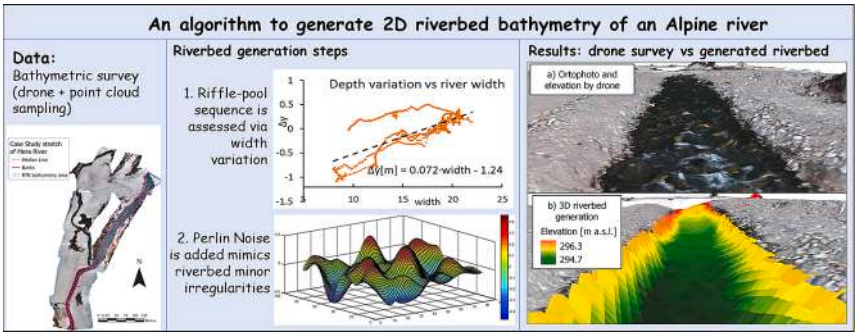

ARTICLE INFO

Editor: José Virgílio Cruz

Keywords:
Hydraulic modelling
2D riverbed generation
Habitat suitability
Perlin noise

ABSTRACT

Here we present an original approach to generate 2D high detail riverbed based on a drone photogrammetric survey, and RTK bathymetry measurements for Mera river in the Italian Alps. The aim is to better represent macro-roughness and riverbed structure of the river, also extending it to an ungauged area. Specifically, we apply a step-by-step approach. I) Depth and average slope of the riverbed were calculated from bathymetry data. II) Thus, a trapezoidal channel with constant slope and variable width was defined using the drone images. III) Riffle-pool sequence was assessed as a function of river width and applied to the generated channel. IV) Finally, the semi-random Perlin Noise was added to recreate riverbed irregularities in the natural stream. HEC-RAS 2D hydraulic software was then implemented to assess spatialized water depth and velocity. The proposed methodology could be quite relevant in river hydraulics to decouple roughness coefficient from water submergence, and in Physical Habitat Simulation Model (PHABSIM), where the dependency of the output is not linear with hydraulic parameters (i.e. water depth and velocity). Indeed, we apply PHABSIM for a case study of a stretch of the river and results are compared with a previous environmental study for Mera river.

* Corresponding author.
E-mail address: davide.fugazza@unimi.it (D. Fugazza).

https://doi.org/10.1016/j.scitotenv.2024.170703
Received 24 July 2023; Received in revised form 24 January 2024; Accepted 3 February 2024
Available online 5 February 2024

1. Introduction

1.1. Potentials of 2D hydraulic modelling and necessary input data

The diffusion of user-friendly and open source 2D hydraulic models, like River2D (Steffler et al., 2002) or HEC-RAS 2D (Brunner et al., 2015), combined with still considerably growing computational power (Andrae, 2020), has led to increasing popularity of 2D models compared to 1D ones. This trend is clearly justified by the higher potential, and the wider fields of application provided by the former (e.g. Teng et al., 2017). Indeed, 2D modelling became crucial in a main field of hydraulic research, i.e. flood analysis (Costabile et al., 2015). While river flow confined within a main, narrow bed can be considered as a 1D system, during overflow, or within geometrically complex channels such as braided streams, depth and velocity fields are largely variable in space, and the hypothesis of 1D flow is no longer valid (Williams et al., 2016). 1D assumption also fails in presence of islands (e.g. Horvat et al., 2020), high sinuosity (e.g. Boano et al., 2006), and in all cases where flow direction needs to be considered. Furthermore, there are circumstances when, even if 1D motion hypotheses are satisfied, it could still be worth applying a 2D model. This occurs when spatialized, and detailed hydraulic parameters are required. In the field of Habitat Suitability Assessment, optimal niches can change even along a section, as fish are very sensitive to local changes in depth, velocity, and substrate (e.g. Jowett and Duncan, 2012).

Nevertheless, the scale of detail of output variables that 2D modelling can provide comes at a price: input data need to be at least equally detailed, pending poor results. While UAVs (unmanned aerial vehicles) can provide digital elevation models of the given terrain with sub-centimeter resolution (e.g. Roni et al., 2019), and thus a flood plain can be described with very high level of detail, the same measurements are very hard to perform in river beds. Here, the electromagnetic signal generated by the drone is either reflected by the water surface, or strongly attenuated, especially under turbid water conditions (e.g. Lee et al., 2022). So, generally for large navigable rivers, bathymetric measurements are performed using a boat equipped with an echo sounder, providing high resolution, but time-consuming measurements. In the case of small non navigable streams, the task is even harder as an operator needs to directly measure elevation of the riverbed with a GPS equipped rod, i.e. performing measurements point by point, and drastically affecting both the resolution and duration of the survey. That said, it is easy to understand why coupling between 1D and 2D models is often considered a good compromise solution: within the river banks, where a certain number of sections are to be measured, a 1D model can be used, while in the floodplain 2D modelling can be applied (Leandro et al., 2009). This hybrid solution is quite often used in the analysis of floods, where the flow geometry as we said turns into bidimensional only after surpassing a threshold discharge, but clearly it is not suitable when a highly detailed solution is necessary even within the main channel.

1.2. Riverbed generation techniques

In recent years, to bypass the limitations to 2D hydraulic modelling

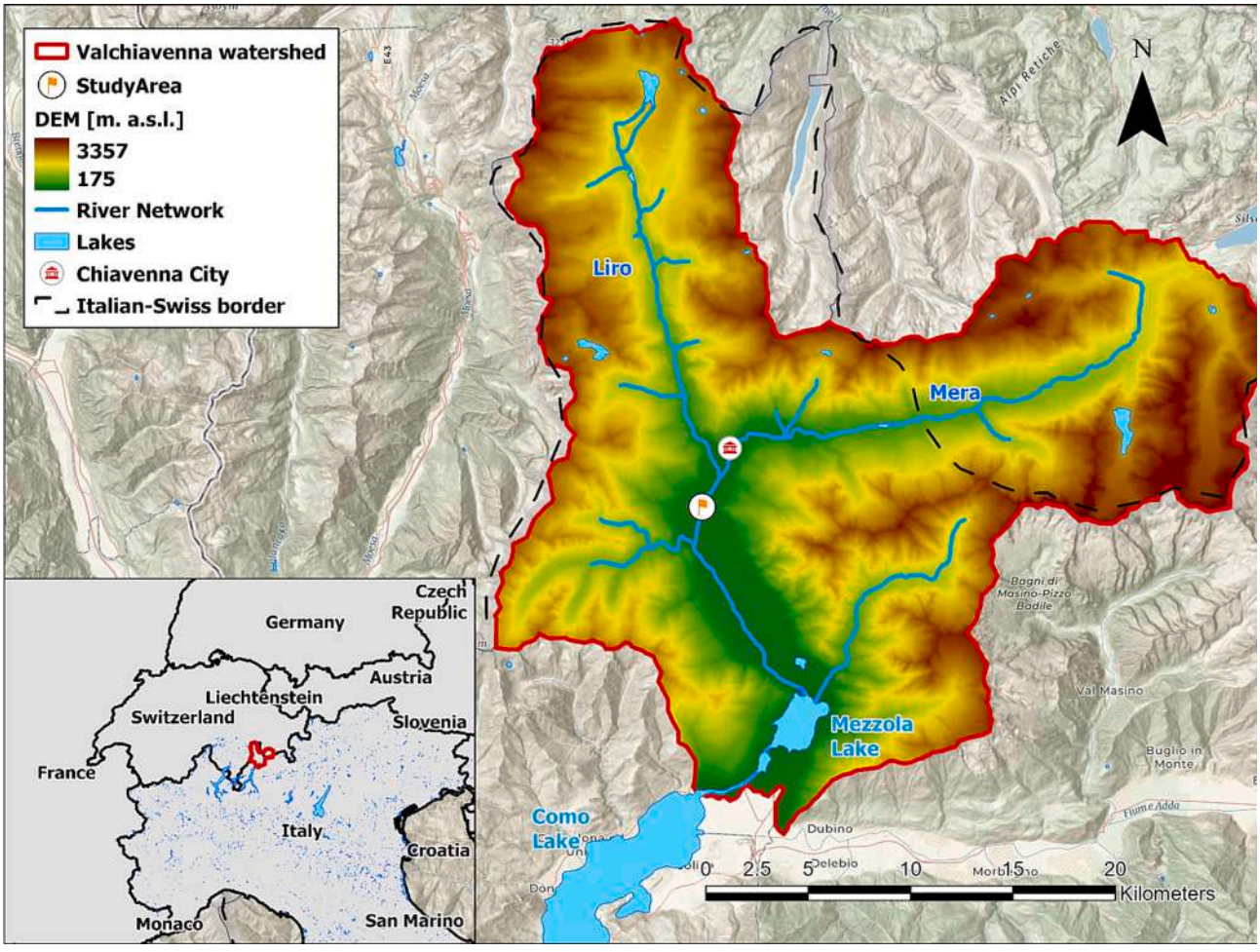

Fig. 1. The transboundary basin of Valchiavenna between Italy and Switzerland. Main rivers, i.e. Liro and Mera, and lakes, i.e. Como and Mezzola, are also reported. Coordinate system WGS84.

with lacking/scarce bathymetric data, some techniques were developed to reconstruct riverbed altimetry. In the worst scenario where no bathymetry is available one can use properly refined Digital Elevation Models, where surrounding topography is used to predict river channel features (Bures et al., 2019). In the presence of bathymetric data, the reconstruction is more easily achievable. A most simple methodology, that can be applied in a regular channel where some data are available (e.g. depth of the thalweg, bank slope) is to generate a trapezoidal channel with constant slope, overlapping the unknown real river path (e.g. Stucchi et al., 2021). When river geometry is more variable, and (enough) dense cross sections are available, the latter can go through transformation from a cartesian coordinate system to a curvilinear one, to interpolate 2D riverbed altimetry (e.g. Song et al., 2020; Caviedes-Voullième et al., 2014). The accuracy of such reconstructed altimetry is largely affected by the morphology of the terrain (Aguilar et al., 2005), i.e. it is most inaccurate for canyon or mountain areas with largest irregularity. Secondarily, it is affected by sampling point density, and eventually by the choice of the interpolation method. As the first two conditions often represent a boundary condition for the designer, most of the effort is focused on the choice of the interpolation method. The most adopted method is linear interpolation (e.g. Merwade et al., 2008), where, to take into account the slope and the variable width of the river, distance in the cross-wise direction is normalized. IDW and Kriging are also quite common, and found to be consistent (Genchi et al., 2020), but splines (e.g. Flanagin et al., 2007) and Natural Neighbour (Bio et al., 2020) have also been reported in literature. Depending upon the considered river, these methods could be more or less representative, and they provide better results with a more regular river, where changes between the sections are mild. For mountain rivers, where areas of riffles and pools can alternate quickly, a large number of river sections would be needed. Furthermore, the composition of the riverbed is often times characterized by the presence of boulders and large rocks, which strongly affects the geometry of the section, making it unusable for interpolation. Lastly, floods are more frequent in mountain rivers, and solid transport is large; thus, river path and width undergo periodic changes in geometry, and measurements rapidly become unreliable and outdated. Thus, in this context the researchers may be forced to give up depiction of the real river pointwise, and turn to a model where general features of the river (riffle-pool sequence, irregular riverbed) are globally preserved, even if mapped bed is not locally accurate.

Here we propose a new methodology to generate the 2D riverbed of an alpine river, where ground bathymetric data are used to relate oscillations of altimetry (riffle-pool sequence) to river local width, allowing the user to generate riverbed depth by remote sensing data, i.e. banks position, extending it to the ungauged area. Furthermore, riverbed irregularities are generated applying a semi-random noise, i.e. Perlin Noise, where spatially correlated oscillations mimic the presence of boulders, and local pools typical of alpine rivers. This generated bathymetry is finally fed to HEC-RAS 2D model to assess the effects of the Perlin Noise on the hydraulic parameters (depth and velocity) for the case study, i.e. Mera river. Finally, a Habitat Suitability Assessment is performed for a series of target fish species.

1.3. Study area

Valchiavenna is an alpine valley of 574 km^2, extending over two regions of two different countries, i.e. Lombardy region in the Italian part, and Canton of Graubunden of Switzerland in its Eastern branch, namely Bregaglia Valley, where Mera river originates (Fig. 1). Downstream of Chiavenna City, the main town of the valley, Mera receives the water from the tributary originated in the Western branch of Valchiavenna, i.e. Liro river of Spluga Valley. Finally, Mera river flows into Lake Como as a second tributary, after Adda river. A recently finished project called GERIKO-MERA (2018–2023) aimed at studying water resources (see Carletti et al., 2022) in the valley, and related issues such as pasture productivity (Casale and Bocchiola, 2022), soil erosion (Maruffi et al., 2022), and river habitat (Salmaso et al., 2021). Many aquatic and terrestrial species build the Mera river habitat, also including the sole otter community within the Italian Alps (Gerosa, 2023), pointing to a decent ecological state of the river, still to be improved according to the Water report by the Regional Environmental Protection Agency of Lombardy (ARPA, 2020). The most valuable fish species of the region, fishing of which is regulated, are brown and marble trout (*Salmo trutta*), grayling (*Thymallus thymallus*), and the European bullhead (*Cottus gobio*).

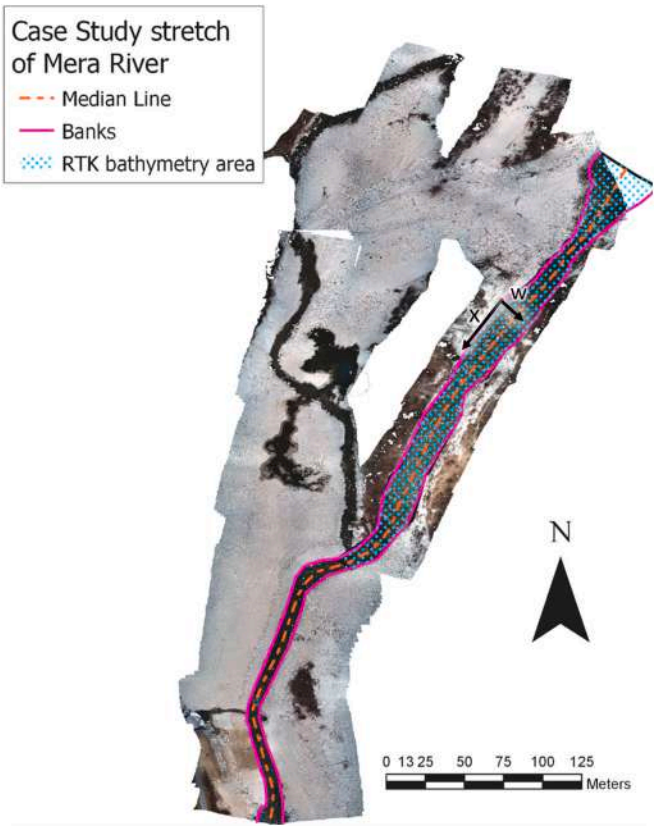

Fig. 2. Case study area: a stretch of ca. 450 m of Mera River. Drone ortophoto with 1 cm resolution, is represented as background image. Bathymetric measurements were performed for ca. 270 m in the upstream part along the major branch.

2. Data and methods

2.1. In situ data

On 11th March 2022, a joint team of researchers from University of Milan, Politecnico di Milano, and University of Insubria, performed the following field measurements on a stretch of Mera river.

2.1.1. Drone data

In order to create a Digital Elevation Model (DEM), and orthophoto of the stretch of Mera river, 941 images were acquired using a DJI Phantom 4 RTK drone. The drone was flown at an altitude of 25 m from take-off, the maximum allowed flying height in the area. Flights were performed manually to avoid running into power grid lines, trees and other obstacles. These circumstances led to a few gaps in areas where trees taller than 25 m were present (white holes in Fig. 2). On the other hand, the low flying altitude allowed obtaining a high spatial resolution of the resulting products. The images were acquired in automatic shooting mode with shutter priority. Shutter speed was 1/1000 s., with

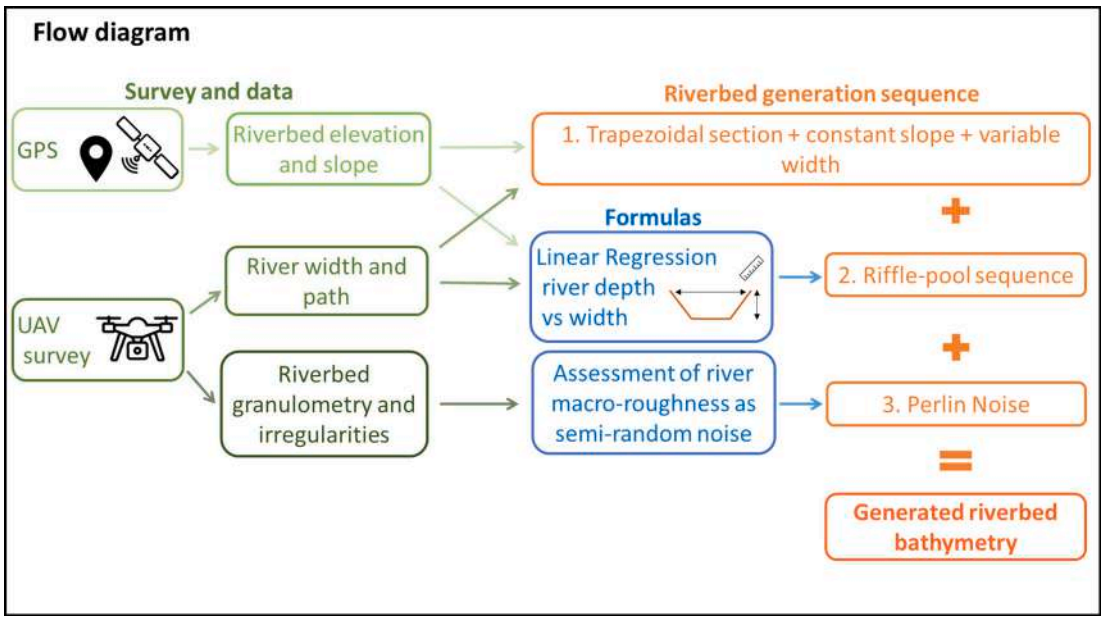

Fig. 3. Flow diagram reporting data processing and algorithm for riverbed bathymetry generation.

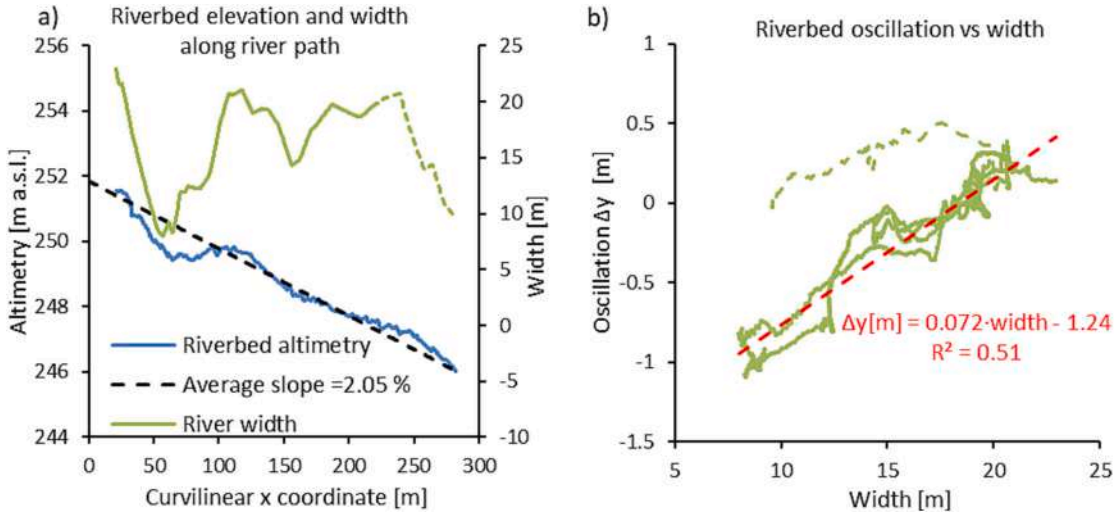

Fig. 4. a) Riverbed elevation profile and river width along measurements area. b) Linear regression between riverbed oscillation and river width.

F-Stop ranging between f/2.8 and f/6.3 and ISO between 100 and 200.

Since no network connection was available in the area for RTK geolocation, before the survey five ground control points made from natural targets (tree branches) were distributed across the survey area to be used as Ground Control Points (GCPs), and aid in the geolocation of the photogrammetric block. Their position was recorded with a Emlid Reach RS GNSS receiver, operating in fast static mode. Processing of the GCP location was performed using Leica Infinity, with the closest available station from the SPIN GNSS network used as a base for differential corrections.

Processing of the photos was carried out using Agisoft Metashape version 1.8.5, following a standard photogrammetric pipeline. Medium accuracy settings were used in both the tie-point extraction/generation of a sparse point cloud, and in the point cloud densification step, while leaving other parameters as default. The five GCPs were used to perform bundle adjustment of the photogrammetric block, and their residual root mean square error was of 8 cm. Finally, the DEM and orthophoto were generated, with a pixel size of 5 cm and 1 cm, respectively.

2.1.2. *Bathymetric data*

Network Real-Time Kinematic (NRTK) Global Navigation Satellite System (GNSS, Leica GS16) samplings were performed in submerged wadable area, which were then post-processed with the software CloudCompare Version 2.6.1., providing a cloud with the altimetry of over 1170 scattered points of the riverbed with a sampling density of 0.21 points for m^2.

2.1.3. *Hydraulic measurements*

As evident in Fig. 2, the upstream part of Mera River is divided into two branches, and the bifurcation starts ca. 80 m away from the study area. Discharge measurements were performed using both a flow tracker, and saline tracer (e.g. using a conductivity meter and sea salt, see e.g. Tazioli, 2011), and it was assessed that discharge of the right branch (referred to an observer looking downstream) is ca. 1/10 of the discharge in the left branch. Moreover, the water depth in the right branch was only few cm at the time of the drone survey, so we decided to consider the drone-derived altimetry as dependable in the right branch,

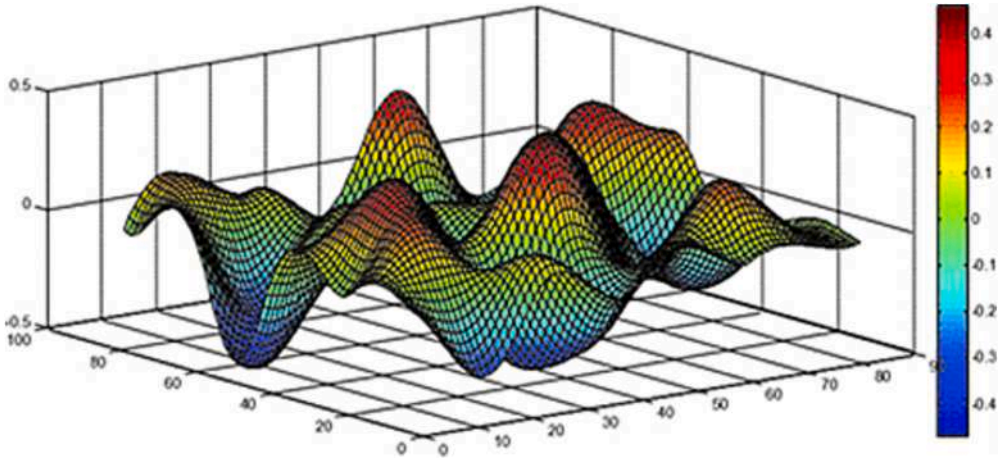

Fig. 5. Example of 2D surface generated with Perlin Noise from Li et al., 2017.

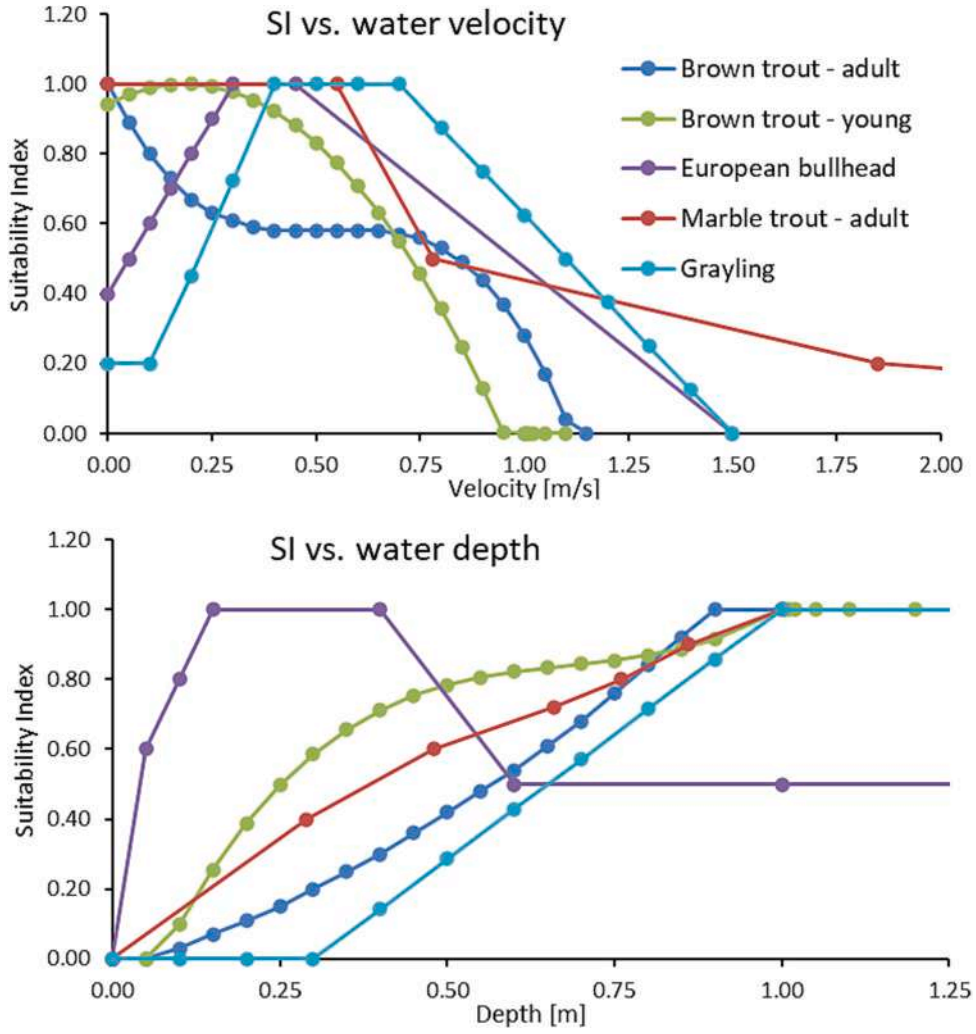

Fig. 6. Habitat Suitability Curves with respect to water Velocity and Depth for 4 fish species: brown trout (young and adult), European bullhead, marble trout, grayling.

and we proceeded to generate riverbed altimetry only for the left branch, both in the area where we have bathymetry, both in the downstream reach after the reconnection where only drone measurements are available.

2.2. Data processing and riverbed generation algorithm

In this section we show how the available data were exploited to define parameters and formula useful to generate the riverbed bathymetry according to the reported algorithm (Fig. 3).

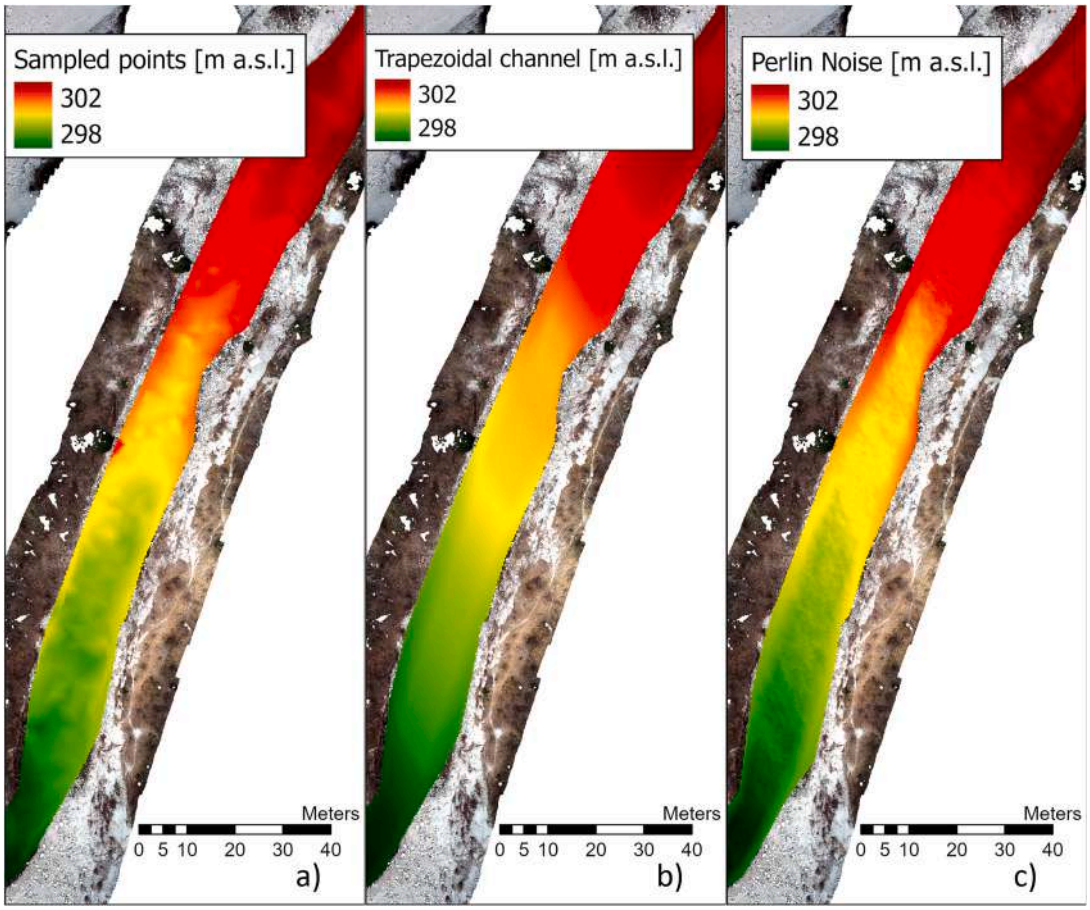

Fig. 7. Riverbed bathymetry generated by a) linear interpolation of sampling points, b) trapezoidal channel from Eq. (1), c) the final output of the model where Perlin Noise is considered.

2.2.1. Curvilinear coordinates system

To describe a river and its structures effectively using a matrix, it is necessary to pass from a Cartesian coordinates system, where points are defined with respect to their longitude and latitude, to a curvilinear one, where points are defined with respect to the river path (x) and width (w) (Fig. 3). First, right and left banks were visually delimited by the operator through GIS software, using as reference wetted area delineated from the orthomosaic generated from the drone images (Fig. 3). These two lines were then subdivided in 1000 equidistant points in the stretch of the river where GPS points of the riverbed were measured, whose length is ca. 285 m, leading to a distance between the vertices of ca. 30 cm. We considered the 1000 segments joining the corresponding points of the banks, and each of these segments was in turn divided into 30 equidistant points leading to the generation of a 1000 × 30 matrix. As the average width of the river is ca. 10 m, the resulting matrix has semi-squared cells (ca. 0.3 × 0.3 m).

2.2.2. Riverbed slope and riffle-pool assessment

We defined local slope of the riverbed exploiting bathymetry measurements: the river centerline was again designed in GIS software, and it was then divided in 1000 points, whose elevation value was defined by considering the nearest bathymetry point (Fig. 4a). We then assessed the oscillation of the riverbed as the difference between measured elevation and theoretical one considering average slope (black dotted line in Fig. 4a). The relevant oscillation owes to the presence of a riffle-pool sequence, that should be also replied when designing riverbed in the downstream area where information about the river is only provided by the orthomosaic map. To do that, we exploit the well-known relationship between the riffle-pool sequence and local banks width (e.g. Carling and Orr, 2000), assessing through Linear Regression riverbed oscillation as a function of the width of the river (red dotted line in Fig. 4b), which is easy to measure from remote sensing data. The fitting is decent except for the last stretch (green dotted line) where the narrowing of the river is not corresponded by a pool sequence. Nevertheless, the shortness of the analysed stretch does not allow a more sophisticated fitting or the use of other parameters like river sinuosity relevant in the formation of riffle-pool sequences (e.g. Richards, 1976).

2.2.3. Trapezoidal channel generation

After assessing the average slope and the equation relating oscillation to river width, it is possible to exploit that relation to model the riverbed depth along the river path as:

$$y(x)\ [m\ a.s.l.] = y_1 - slope \bullet x + \Delta y = 251.8 - 0.0205x + 0.072width(x) - 1.24 \quad (1)$$

where y is the elevation of the riverbed in the considered cell, x is the distance in curvilinear coordinates from the first upstream point x_1 with elevation y_1, Δy is the riverbed oscillation depending on river local *width* as explained above, 251.8 m is initial riverbed elevation for x = 0, −0.0205 is average river slope, and 0.072 and − 1.24 are the coefficients found by Linear Regression in Fig. 3b.

Now we can define a trapezoidal channel, mapping riverbed altimetry using, as altitude values for the banks, those extracted by the DEM generated from drone data. We assign to the bottom of the channel the value of altitude y defined in Eq. (1). As river width varies along the path, we also apply change in river bank slope by keeping constant the proportions between the extension of the left bank, riverbed, and right

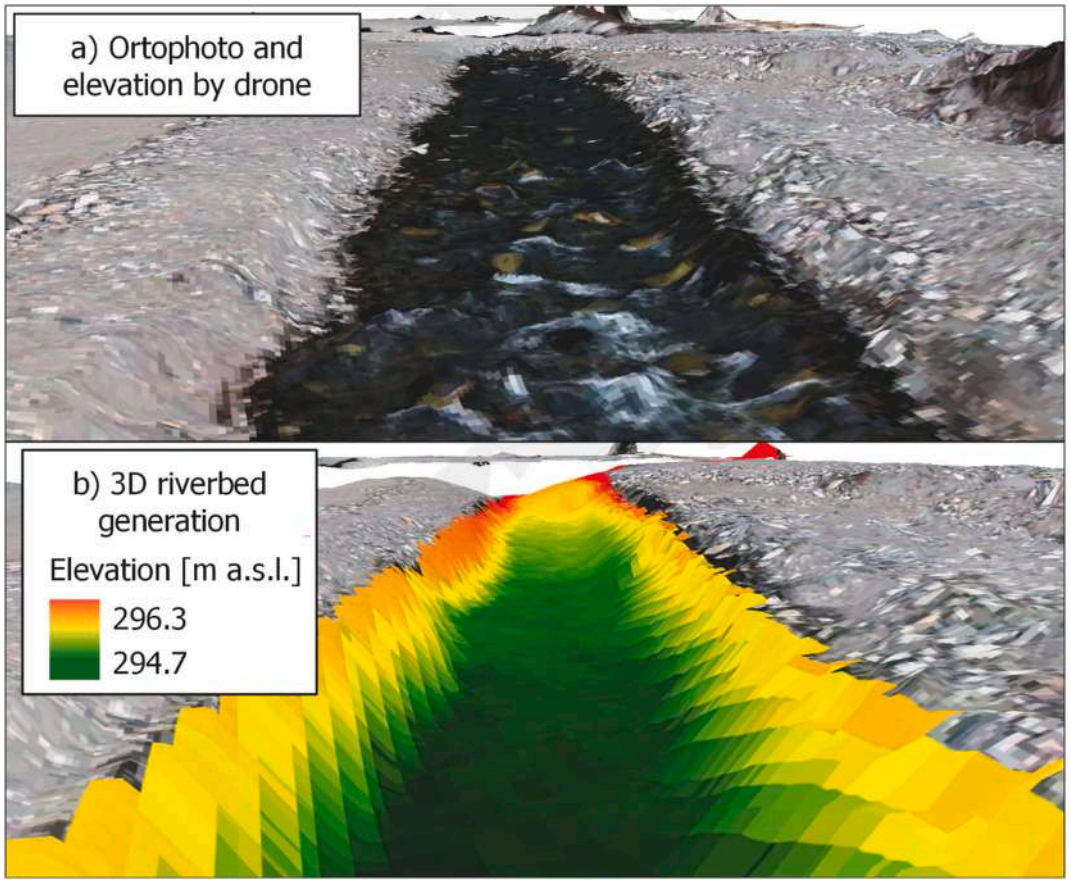

Fig. 8. a) Ortophoto and elevation profile elaborated by drone in March 2022 and b) 2D riverbed generated in this study.

bank, equal to 7/30, 16/30, 7/30 respectively. This leads to a variable bank slope according to the width of the channel, coherently with what observed during the field campaign, i.e. the highest slope in the narrowest sections, and the lowest in the largest ones.

2.2.4. 2D Perlin noise

Here, we defined a riverbed with constant slope, and variable width and depth. To recreate minor patterns within the riverbed (e.g. local small pools, large boulders, etc), we also added a noise function, i.e. the Perlin noise (Fig. 5). This is a peculiar kind of noise, where generated values are spatially correlated and continuous, and thus suitable to represent natural textures like landscape, clouds, turbulence etc. It was indeed firstly introduced by the computer scientist Ken Perlin (1985), with the specific purpose to create realistic terrain in computer graphics. During the years many formulations were developed in the family of Perlin Noise, which are generally identified by the following steps:

- The generation of random values over a grid (which can be n-dimensional);
- The interpolation of the random values using a function (eg. spline, cubical, etc) at a given step.

This process can be repeated changing the interpolation step to create fluctuations at a given spatial scale. The sum of the generated grids will provide the output grid.

Here, as a first approach we used a spline function to interpolate the random grid, and we lowered the fluctuation generated by Perlin noise through a final passage through a logarithmic function, to keep it as much representative as possible of real river bedrock. Hence, in accordance with the cobble composition of the riverbed and alluvial plain, we accepted a maximum fluctuation of +/− 20 cm. Furthermore, we linearly dampen fluctuations along the banks, because they are generally more regular compared to the river bed. Finally, we add the generated Perlin Noise matrix to the previously mapped trapezoidal channel, to obtain a complete riverbed bathymetry.

2.3. Hydraulic modelling

Here, we used for hydraulic simulation the software HEC-RAS® (Brunner, 2016), in 2-D mode. HEC-RAS 2D solves Shallow Water Equations (SWEs), here simplified with the Diffusion Wave Equation (computation interval 0.2 s), to calculate spatially distributed (here, on a 0.30 m grid) flow depth D, and flow velocity components, Vx and Vy, in two plane directions x and y, respectively. The spatial domain for hydraulic simulation is the one defined by super-imposition of the generated riverbed to the drone altimetry measurement, downscaled to 0.30 m. Strickler's coefficient was fixed to 0.06 [$m^{-1/3}s$] by comparison with literature data for riverbed made of gravel and boulders (Barnes, 1967). We used steady hydrographs, i.e. we implemented HEC-RAS 2-D simulation, until it reached steady state, i.e. no significant variation of flow velocity was detected (as in Stucchi et al., 2021).

We pursued 9 simulations for 9 values of discharge ($Q^* = 1.4, 2, 2.5, 3, 4, 5, 6, 7, 8\ m^3s^{-1}$), chosen between the 4 used in another study on Mera river (Servanzi et al., 2023), plus 5 other values to define a more stable regression vs Habitat Suitability parameters.

We used as boundary conditions for every simulation i) the constant discharge for the two upstream branches ($Q^l = \frac{9}{10}Q^*$ for the left branch, while $Q^r = \frac{1}{10}Q^*$ for the right branch), and ii) uniform (normal) flow depth for the downstream section, with local geometry, and mean slope of the stream (ca. 0.15 %), providing mixed conditions for sub/super critical flows.

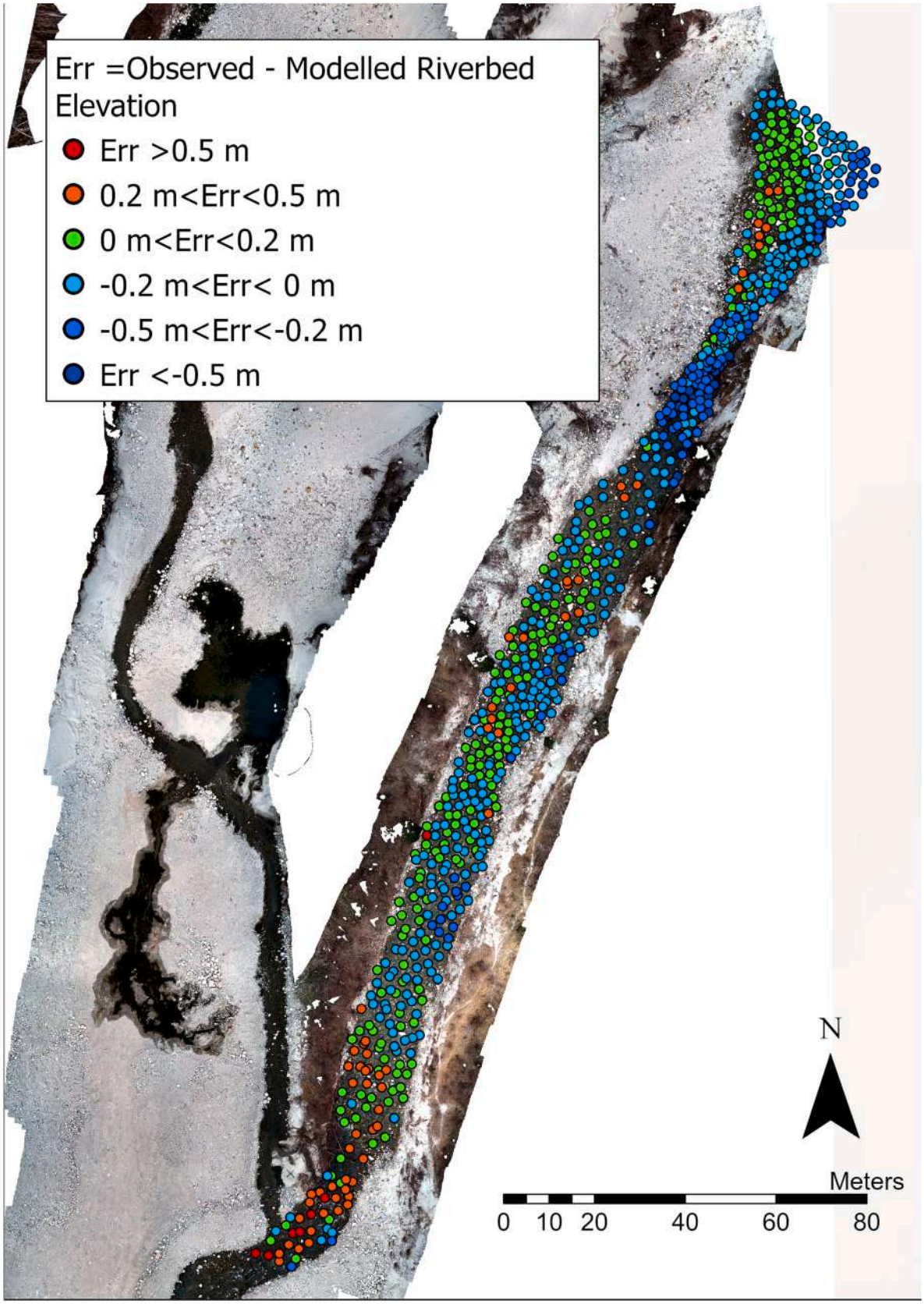

Fig. 9. Comparison of the generated riverbed and measured one. The difference (Err) between observed points and modelled riverbed elevation is reported and clustered in 6 classes.

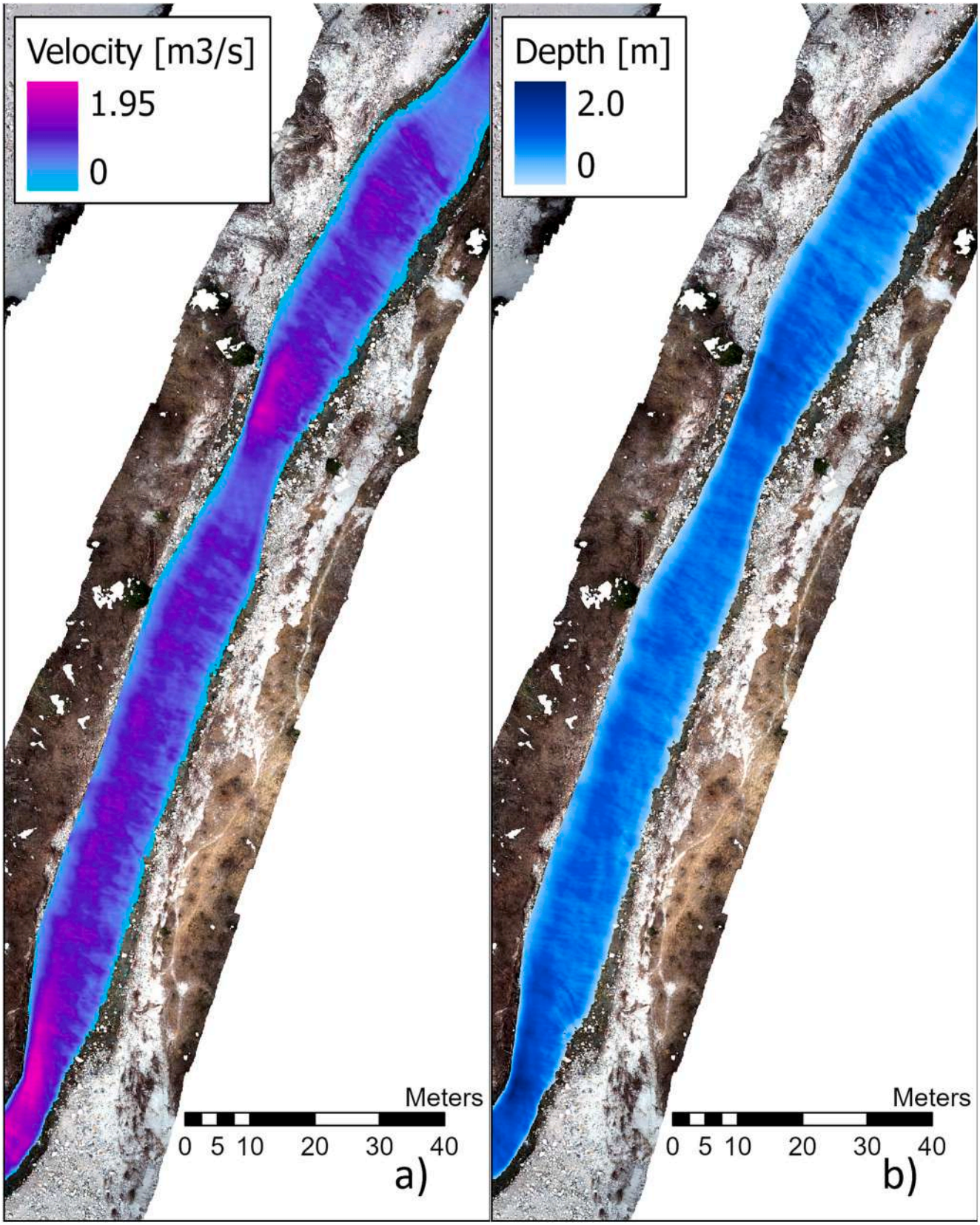

Fig. 10. Water depth and velocity obtained by hydraulic modelling considering Perlin Noise bathymetry and Q = 2.2 m^3s^{-1}.

Table 1
Comparison of hydraulic parameters from different simulations with the following bathymetries: 1 generated with no Perlin Noise, 7 bathymetries with Perlin Noise, whose outputs were averaged and used to assess the Root Mean Square Error.

$Q = 2.2\ m^3s^{-1}$	Velocity [m^3s^{-1}]		Depth [m]	
	Average	RMSE	Average	RMSE
No Perlin Noise	0.55	0.24	0.15	0.08
Perlin Noise 1	0.66	0.08	0.20	0.04
Perlin Noise 2	0.66	0.08	0.20	0.04
Perlin Noise 3	0.66	0.08	0.20	0.03
Perlin Noise 4	0.66	0.09	0.20	0.04
Perlin Noise 5	0.66	0.09	0.20	0.04
Perlin Noise 6	0.66	0.08	0.20	0.04
Perlin Noise 7	0.66	0.08	0.20	0.04
Average Perlin Noise	0.66	–	0.20	–

2.3.1. Habitat suitability curves

According to the IFIM-PHABSIM method (Milhous et al., 1984), we use site specific curves expressing the Suitability Index (SI) with respect to water depth and velocity, i.e. to sketch most preferred hydraulic conditions for the fish (0 not suitable, 1 fully suitable). Here we used the SI for 4 valuable fish species (and two age stages from *Brown Trout*, Fig. 6), computed by Servanzi et al. (2023) from field measurements in a reach 2 km downstream of our case study.

Weighted Usable Volume (WUV), i.e. the volume of water "suitable" for fish, is then assessed for each wet cell of the domain according to the formula:

$$WUV = SI_{depth} \times SI_{velocity} \times D \times l_{cell}^2 \tag{2}$$

where D is water depth and l_{cell} is the size of the cell of the grid (i.e. 0.30 m). Furthermore, we can assess a Weighted Usable Area (WUA), which in 1D PHABSIM is considered equal to the area of the section suitable for fish. Here, for comparison with Servanzi et al. (2023), we consider a particular type of wetted area, namely the horizontal wetted area suitable for colonization, calculated for all the n cells of a stretch, normalized for its length, expressed as

$$WUA = \frac{\sum_{i=1}^{n}\left(SI_{depth,i} \times SI_{velocity,i} \times l_{cell}^2\right)}{length} \tag{3}$$

3. Results

3.1. Riverbed bathymetry generation

To better depict the proposed methodology, and visualize its potentiality, we provide 3 bathymetry maps in Fig. 7: a) the riverbed obtained with the linear interpolation of measured points, b) the trapezoidal channel generated as an intermediate step of the presented procedure (see Section 2.2), and c) the final bathymetry obtained superimposing to the latter the Perlin Noise, where the irregularities encountered in the measured data are to some extent reproduced.

Moreover, we provide a 3D picture of the generated riverbed compared to the one assessed by drone survey, which appears much flatter as it measures water surface elevation, pointing to the need of a modelling procedure (Fig. 8).

We report in Fig. 9 a comparison of the model with measured data, i.e. the *Error* (altitude difference) between the observed riverbed altimetry, and the manually measured points for the main branch of Mera river. Here, the average of the absolute value of the altitude difference is equal to 0.21 m. Specifically, 65 % of the points have an *Error* between ±0.2 m, and 6 % show an *Error* larger than ±0.5 m, which is especially high in the downstream part of the river, where the linear regression equation (Eq. (1)) to detect riffle-pool sequence provides the largest uncertainty (Fig. 4b). Overall, since the algorithm here implemented assesses oscillation due to riffle-pool sequences from −1 to 0.5 m ca. (Eq. (1), Fig. 4b), plus a random fluctuation of maximum −0.2/+0.2 m, the observed *Error* is considered acceptable.

3.2. Hydraulic outputs of Perlin Noise

We report in Fig. 10 the results in terms of water depth and velocity provided using Perlin Noise with a low discharge level, i.e. $Q = 2.2\ m^3s^{-1}$, where the effects of the introduced noise on the hydraulic parameters are more evident. To verify that the specific bathymetry can be considered equivalent with others generated with the same (partially random) approach, we run 7 simulations considering Perlin Noise, checking the congruity of the global results (Table 1). We also consider a bathymetry generated with the same algorithm but with no Perlin Noise (as in Fig. 7b). The simulation with no random fluctuation provides both lower water depth and velocity. As expected Perlin Noise decreases the hydraulic radius and adds extra roughness to the channel, causing higher water level. Furthermore, the presence of macro-irregularities disrupts water flow, which does no longer run parallel to the river path, but diverges where Perlin Noise generates micro-riffles, and converges to the parts where Perlin Noise generates higher depth. This variance of the flow profile causes indeed higher water velocity. On the other hand, generating other random surfaces with Perlin Noise we obtain the same results in terms of average water depth and velocity, but not neglectable variance due to the local differences between the models.

3.3. PHABSIM output

In Table 2, and Fig. 11 we show the main hydraulic parameters, average water depth and velocity, and values of WUV for the considered species. For all the 9 considered values of discharge, no overbank occurs for Mera River. For this reason, we observe the values of depth (and velocity) steadily increasing with no considerable jumps (see Fig. 11a).

Table 2
Values of discharge used for 2D simulations and corresponding values of water depth, velocity and WUV, WUA values normalized respectively for the river wetted area and length.

Q [m^3s^{-1}]	Water depth [m]	Water velocity [m s^{-1}]	WUV·10 [m^3/m] | WUA [m^2/m]				
			Brown trout		European Bullhead	Grayling	Marble trout
			adult	young			
1.5	0.18	0.51	0.2 | 0.8	0.9 | 3.6	1.5 | 7.9	0.5 | 0.2	0.6 | 3.0
2	0.23	0.57	0.4 | 1.4	1.2 | 5.4	1.8 | 10.4	0.9 | 0.9	1.0 | 4.6
2.4	0.25	0.61	0.4 | 1.6	1.3 | 5.8	1.9 | 10.8	1.0 | 1.0	1.1 | 4.9
3	0.29	0.68	0.6 | 2.0	1.5 | 6.3	2.0 | 11.0	1.5 | 1.6	1.3 | 5.4
4	0.34	0.76	0.8 | 2.4	1.7 | 6.8	2.2 | 11.2	1.9 | 2.2	1.5 | 5.8
5	0.39	0.84	1.0 | 2.8	1.8 | 7.0	2.5 | 11.4	2.2 | 2.7	1.7 | 6.2
6	0.43	0.90	1.1 | 3.0	1.8 | 7.1	2.6 | 11.5	2.3 | 3.2	1.9 | 6.6
7	0.45	0.92	1.2 | 3.1	1.8 | 7.1	2.6 | 11.4	2.4 | 3.6	2.1 | 7.0
8	0.48	0.93	1.1 | 3.2	1.9 | 7.4	2.6 | 11.8	2.5 | 3.9	2.2 | 7.6

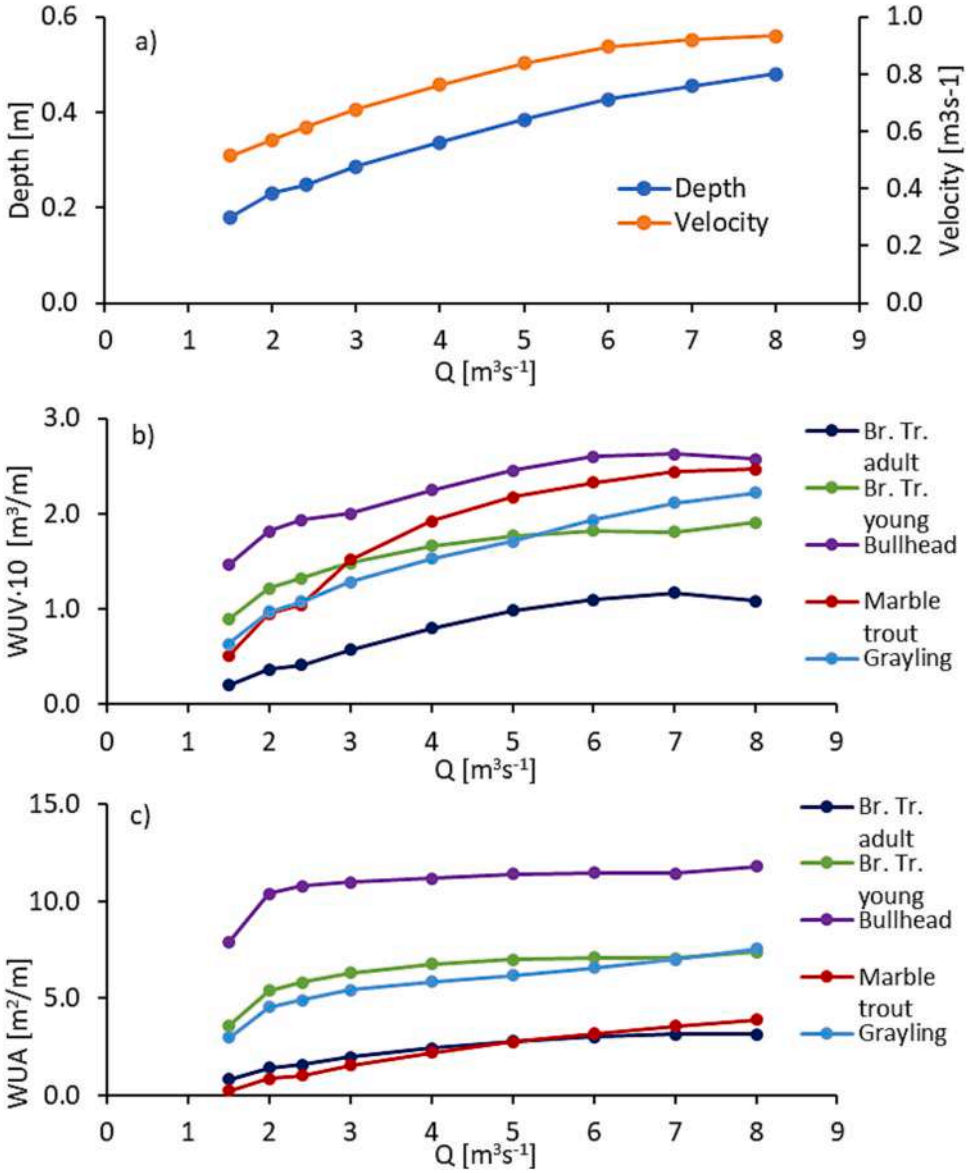

Fig. 11. a) Main hydraulic parameters, e.g. average water depth and velocity for considered discharge values (Q = 1.5, 2, 2.4, 3, 4, 5, 6, 7, 8 m^3s^{-1}). b) Weighted Usable Volume and c) Weighted Usable Area values (normalized with respect to wet area and reach length, respectively) for the considered species: Brown Trout (adult and young), European Bullhead, Marble trout (adult), Grayling.

On the other hand, with the exception of grayling, for the considered species WUV is not growing largely above Q = 6 m^3s^{-1} ca., and it is even (marginally) decreasing (Fig. 11b). WUA curves behave similarly to WUV, but since variation in wetted area are smaller than changes in water depth, the WUA curves are also flatter (Fig. 11c).

As we mentioned, in a recent study (Servanzi et al., 2023) under the framework of the GERIKO-Mera project, Habitat Suitability was analysed for a stretch of ca. 400 m, located 2 km downstream of our case study area. Also there WUA was assessed, and our results are benchmarked against that study in Fig. 12.

In our study area, WUA seems consistent with those in Servanzi et al. (2023), albeit slightly lower for each discharge and species, except for the *Bullhead*. This may be a result of the different slope of the two stretches, i.e. 0.3 % therein, and 2 % here. This difference would result into lower water depth in our stretch, which indeed represents an asset for the bullhead (Fig. 6). On the other hand, our estimated WUA seems (much) lower for species preferring relatively high water depth, such as *brown trout* (both young and adult). This difference seems more pronounced in case of low discharges, which may put under further stress the fish, with respect to (low) water depth conditions.

4. Discussion

4.1. Why to prefer a generated riverbed bathymetry compared to a measured one

The algorithm here designed aims to realistically mimic the bathymetry of a natural riverbed, taking into account the riffle-pool sequence, relating it to the river width, and also considering the natural ruggedness of the bedrock, with the spatially correlated Perlin Noise. While considering the riffle-pool sequence increases the accuracy of the generated bathymetry (except for the downstream area where linear regression provides large uncertainty), the addiction of random noise actually decreases the punctual solidity of the model. Nevertheless rivers, especially in alpine areas, undergo periodic change in the riverbed shape because of solid transport, with the result of nullifying any effort to reproduce point to point the geometry of the river. Therefore it is more relevant to replicate the general river structure, i.e.

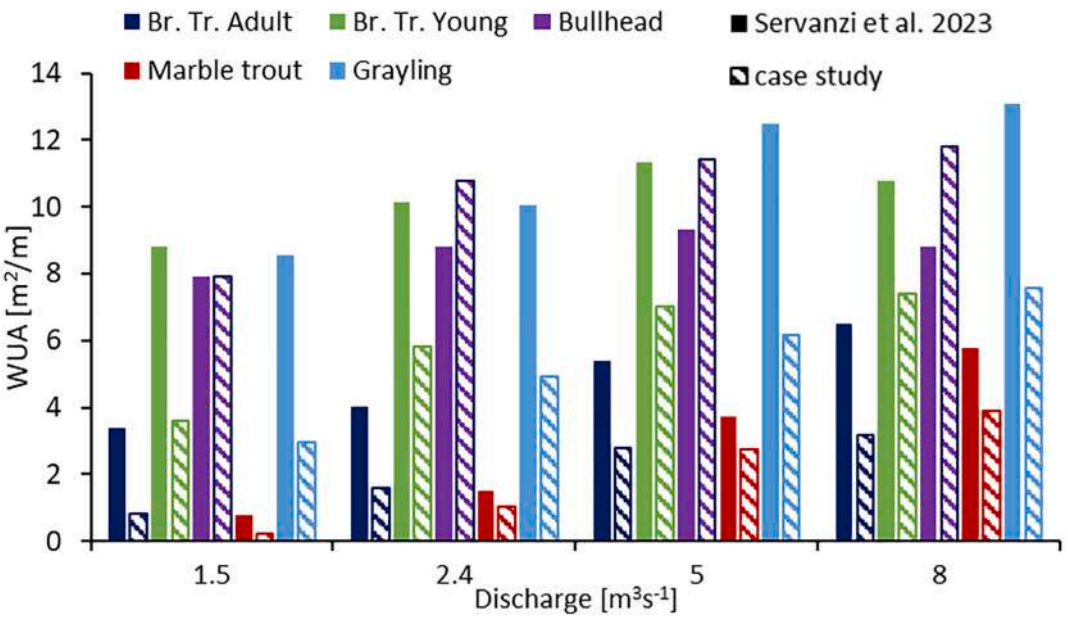

Fig. 12. Results in term of WUA normalized for reach length in Servanzi et al. (2023) vs. case study area here analysed.

the presence of riffle-pool sequences and irregularities caused by boulders, which affect the hydraulic parameters.

4.2. The effects of additional macro-roughness (Perlin Noise) on hydraulic parameters

As we showed in Table 1, the presence of irregularities, here replicated with Perlin Noise, will lead to very minor changes in wetted area A_w (by adding, and subtracting similar pieces of area), but to increased wetted perimeter P_w, for the same water level. This in turn, according to the Chezy equation, leads to a lower hydraulic radius (defined as the ratio between wetted area, and wetted perimeter $R = A_w/P_w$). Also bed roughness will increase (i.e. Manning's n increases). Manning's coefficient (Manning, 1891) would be independent of water stage, unlike the Gauckler-Strickler coefficient (1867), however at the cost of being multiplied by the hydraulic radius raised to a power of *1/6*

$$Q = \frac{1}{n}R^{\frac{1}{6}}\sqrt{R^{\frac{1}{3}}slope}A_w = \frac{1}{n}R^{\frac{2}{3}}\sqrt{slope}A_w = \frac{1}{nP_w^{\frac{2}{3}}}\sqrt{slope}A_w^{\frac{5}{3}} \quad (4)$$

Accordingly, the more rugged the bottom (n,P_w increase), the higher flow area (A_w and depth, depending upon geometry) will be necessary to convey a certain discharge.

The *1/6* exponent was in turn only recently theoretically validated by Gioia and Bombardelli (2001) based upon a phenomenological theory of turbulence. Despite such, Manning's coefficient being a dimensional quantity ($m^{-1/3}s$), it cannot be defined as a scale invariant quantity of the system, even in a fully developed turbulent regime where auto-similarity of the system has been well known for more than a century (Richardson, 1922).

In mountain streams, often times the water stage is equal to, or lower than the size of the largest rocks within the riverbed, and such elements make flow regime assessment less viable when using the high submergence hypothesis (Nikora et al., 2001). Accordingly, many formulations were introduced in literature to consider the variability of Manning's coefficient in low submergence case. Limerinos (1970), and Colosimo et al. (1988) assessed the variability of the friction coefficient considering submergence level, with respect to roughness of the river bottom, e.g. considering higher values of Manning's coefficient for low submergence flow regimes.

4.3. Present limitations, and potential outlooks for the use of Perlin Noise in river hydraulic

As mentioned, the addition of Perlin Noise results into higher resistance (higher n, lower R) for low flow regimes, and thus it may be worth further investigation of the topic, as to how the Manning's coefficient should change to obtain the same water depth as with the addition of Perlin Noise. A most relevant perspective would be to use a proper defined Perlin Noise function and bypass the aforementioned formulations to face the matter of the variability of Manning's coefficient with respect to submergence level.

Water velocity obtained with Perlin Noise on the other hand could be to replicate, as we saw that Perlin Noise increases both the water depth and the water velocity, where the velocity profile is no more parallel to the river path, leading to discrepancies with velocity values simulated with regular riverbed, which in turn may lead to different *Suitability Index* and WUA/WUV. A solution to this problem, here not applied, could be to consider only the velocity component parallel to flow direction, that is the variable actually considered by the operators when measuring in situ river velocity and discharge.

Here Perlin Noise was defined, only considering a maximum oscillation value, but several variations were developed according to the surface of interest (e.g. Dustler et al., 2015; Michot-Roberto et al., 2021). A further development here may entail use of different Perlin Noise methods, as well as a detailed sensitivity analysis of the output of the hydraulic model. With this refinement potentially, specific Perlin Noise functions could be used to mimic each riverbed material, that can generally be assessed with satellite images, online pictures, public reports, etc.

4.4. Synthetic riffle-pool sequence generation: Limitations and outlooks

The algorithm here presented also relates riffle-pool sequence to local river width by linear regression, although the development of these sequences is a complex theme, and a main focus in literature (e.g. Langbein and Leopold, 1964; Gregory et al., 1994). In particular, it is ascertained that their morphology depends on river slope, sediment composition, sinuosity, and, in addition to the local value, it also depends on downstream river width (Chartrand et al., 2023). Nevertheless, lack of extended data led us to consider a simple linear regression with respect to only 1 variable, but the formula could be made more refined,

and dependable extending the analysis to other Alpine rivers, and possibly including in the formulation river slope, which can also be estimated using remote sensing.

5. Conclusions

A new method to generate detailed riverbed topography of a river was presented here. A point cloud of riverbed bathymetry, and a DEM derived from a drone survey provided the background to calibrate and validate a general algorithm for riverbed generation, which was also extended within an unmeasured stretch of the river. Indeed, while literature models to create riverbed are based on interpolation algorithms, and thus are generally limited by the presence of measured sections/point clouds, the algorithm here developed has the potential to mimic riverbed altimetry everywhere, keeping a more consistent, even though pointwise less accurate, terrain texture. This includes use of a semi-random Perlin Noise function, which was here applied for the first time in a hydraulic study. The results provided by the algorithm shows a small error compared to the measured riverbed bathymetry, mainly due to the approximated estimation of riffle-pool sequence provided by the model. The method, adding macro-roughness to the riverbed, could help to bypass the problem of the variability of the Manning coefficient with respect to submergence level. As a further example of application, we consider PHABSIM, where Habitat Suitability is not linear with hydraulic parameters, and thus adding a zero average noise could lead to non-zero variations.

The preliminary algorithm designed here seems of interest, and with a proper refinement in other case studies it could provide a general method to apply 2D hydraulic modelling in ungauged areas, useful for hydraulic, ecological, and morphological studies, for scientists, and (water) policy makers.

CRediT authorship contribution statement

L. Stucchi: Writing – original draft, Software, Methodology, Formal analysis, Conceptualization. **D. Fugazza:** Writing – review & editing, Formal analysis, Data curation. **A. Sharifi:** Software, Formal analysis. **G. Traversa:** Writing – review & editing, Data curation. **G. Diolaiuti:** Supervision, Project administration. **D. Bocchiola:** Writing – review & editing, Supervision, Methodology.

Declaration of competing interest

The authors declare that they have no known competing financial interests or personal relationships that could have appeared to influence the work reported in this paper.

Data availability

Data will be made available on request.

Acknowledgments

The results presented in this work are in fulfilment of the Interreg project GE.RI.KO Mera (EU INTERREG ITALIA-SVIZZERA 2014/2020) coordinated by Comunità Moontana di Valchiavenna (SO), kindly acknowledged. The authors kindly acknowledge support from the project partners Dr. Livia Servanzi and prof. Paolo Espa who shared the precious data of riverbed bathymetry surveys. Support from *Climate_Lab*, the interdisciplinary laboratory on climate change at Politecnico di Milano (https://www.climatelab.polimi.it/en/) is kindly acknowledged.

References

Aguilar, F.J., Agüera, F., Aguilar, M.A., Carvajal, F., 2005. Effects of terrain morphology, sampling density, and interpolation methods on grid DEM accuracy. Photogramm. Eng. Remote Sens. 71 (7), 805–816.

Andrae, A.S., 2020. Hypotheses for primary energy use, electricity use and CO2 emissions of global computing and its shares of the total between 2020 and 2030. WSEAS Transactions on Power Systems 15 (50–59), 4.

ARPA Lombardy (2020). "State of surface water in Lombardy. Mezzola Lake. 2014-2019 update. Environmental Monitoring", Pag 21. Available in Italian on ARPA website at: https://www.arpalombardia.it/media/xqhprzlh/rapporto_2014_2019_mezzola.pdf.

Barnes, 1967. Roughness Characteristics of Natural Channels. Department of the Interior. U.S. Geological Survey.

Bio, A., Gonçalves, J.A., Magalhães, A., Pinheiro, J., Bastos, L., 2020. Combining low-cost sonar and high-precision global navigation satellite system for shallow water bathymetry. Estuar. Coasts. https://doi.org/10.1007/s12237-020-00703-6.

Boano, F., Camporeale, C., Revelli, R., Ridolfi, L., 2006. Sinuosity-driven hyporheic exchange in meandering rivers. Geophys. Res. Lett. 33 (18).

Brunner, G.W., 2016. HEC-RAS River analysis system, reference manual. Davis US Army Corps Eng. Hydrol. Eng. Cent. 75.

Brunner, G.W., Piper, S.S., Jensen, M.R., Chacon, B., 2015. Combined 1D and 2D hydraulic modeling within HEC-RAS. In: World Environmental and Water Resources Congress 2015, pp. 1432–1443.

Bures, L., Sychova, P., Maca, P., Roub, R., Marval, S., 2019. River bathymetry model based on floodplain topography. Water 11, 1287. https://doi.org/10.3390/w11061287.

Carletti, F., Michel, A., Casale, F., Burri, A., Bocchiola, D., Bavay, M., Lehning, M., 2022. A comparison of hydrological models with different level of complexity in alpine regions in the context of climate change. Hydrol. Earth Syst. Sci. 26 (13), 3447–3475. https://doi.org/10.5194/hess-26-3447-2022.

Carling, P.A., Orr, H.G., 2000. Morphology of riffle–pool sequences in the river Severn, England. Earth Surf. Process. Landforms 25 (4), 369–384. https://doi.org/10.1002/(SICI)1096-9837(200004)25:4<369::AID-ESP60>3.0.CO;2-M.

Casale, F., Bocchiola, D., 2022. Climate change effects upon pasture in the Alps: the case of Valtellina Valley, Italy. Climate 10 (11), 173. https://doi.org/10.3390/cli10110173.

Caviedes-Voullième, D., Morales-Hernández, M., López-Marijuan, I., García-Navarro, P., 2014. Reconstruction of 2D river beds by appropriate interpolation of 1D cross-sectional information for flood simulation. Environ. Model. Software 61, 206–228. https://doi.org/10.1016/j.envsoft.2014.07.016.

Chartrand, S.M., Jellinek, A.M., Hassan, M.A., Ferrer-Boix, C., 2023. Coupling between downstream variations of channel width and local pool–riffle bed topography. Earth Surf. Dyn. 11 (1), 1–20. https://doi.org/10.5194/esurf-11-1-2023.

Colosimo, C., Copertino, V.A., Veltri, M., 1988. Friction factor evaluation in gravel-bed rivers. J. Hydraul. Eng. 114 (8), 861–876. https://doi.org/10.1061/(ASCE)0733-9429(1988)114:8(861).

Costabile, P., Macchione, F., Natale, L., et al., 2015. Flood mapping using LIDAR DEM. Limitations of the 1-D modeling highlighted by the 2-D approach. Nat. Hazards 77, 181–204. https://doi.org/10.1007/s11069-015-1606-0.

Dustler, Magnus, Bakic, Predrag, Petersson, Hannie, Timberg, Pontus, Tingberg, Anders, Zackrisson, Sophia, 18 March 2015. Application of the fractal Perlin noise algorithm for the generation of simulated breast tissue. In: Proc. SPIE 9412, Medical Imaging 2015: Physics of Medical Imaging, 94123E. https://doi.org/10.1117/12.2081856.

Flanagin, M., Grenotton, A., Ratcliff, J., Shaw, K.B., Sample, J., Abdelguerfi, M., 2007. Hydraulic splines: a hybrid approach to modeling river channel geometries. Comput. Sci. Eng. 9 (5), 4–15.

Gauckler, Ph., 1867. Etudes Théoriques et Pratiques sur l'Ecoulement et le Mouvement des Eaux, vol. Tome 64. Comptes Rendues de l'Académie des Sciences, Paris, France, pp. 818–822.

Genchi, S.A., Vitale, A.J., Perillo, G.M., Seitz, C., Delrieux, C.A., 2020. Mapping topobathymetry in a shallow tidal environment using low-cost technology. Remote Sens. (Basel) 12 (9), 1394. https://doi.org/10.3390/rs12091394.

Gioia, G.; Bombardelli, F. A. (2001). "Scaling and similarity in rough channel flows". Phys. Rev. Lett. 88 (1): 014501. doi:https://doi.org/10.1103/PhysRevLett.88.014501)https://doi.org/10.1103/PhysRevLett.88.014501).

Gerosa, B., 2023. La lontra torna in Valchiavenna: era sparita dall'Italia per la caccia e i cambiamenti climatici. Corriere della Sera. Available in Italian at: https://milano.corriere.it/notizie/lombardia/23_marzo_14/la-lontra-torna-in-valchiavenna-era-sparita-dall-italia-per-la-caccia-e-i-cambiamenti-climatici-b2f2da73-b31a-4cdc-bcdf-7e7a61d0cxlk.shtml.

Gregory, K.J., Gurnell, A.M., Hill, C.T., Tooth, S., 1994. Stability of the pool-riffle sequence in changing river channels. Regul. Rivers: Res. Mgmt. 9, 35–43. https://doi.org/10.1002/rrr.3450090104.

Horvat, Z., Horvat, M., Majer, F., et al., 2020. Hydraulic analysis of a meander on the Danube River using a 2D flow model. Environ. Monit. Assess. 192, 149. https://doi.org/10.1007/s10661-020-8074-z.

Jowett, I.G., Duncan, M.J., 2012. Effectiveness of 1D and 2D hydraulic models for instream habitat analysis in a braided river. Ecol. Eng. 48, 92–100. https://doi.org/10.1016/j.ecoleng.2011.06.036.

Langbein, W.B., Leopold, L.B., 1964. Quasi-equilibrium states in channel morphology. Am. J. Sci. 262 (6), 782–794.

Leandro, J., Chen, A.S., Djordjević, S., Savić, D.A., 2009. Comparison of 1D/1D and 1D/2D coupled (sewer/surface) hydraulic models for urban flood simulation. J. Hydraul. Eng. 135 (6), 495–504. https://doi.org/10.1061/(ASCE)HY.1943-7900.0000037.

Lee, C.H., Liu, L.W., Wang, Y.M., Leu, J.M., Chen, C.L., 2022. Drone-based bathymetry modeling for mountainous shallow rivers in Taiwan using machine learning. Remote Sens. (Basel) 14 (14), 3343. https://www.mdpi.com/2072-4292/14/14/3343.

Li, H., Yang, H., Xu, C., Cao, Y., 2017. Water surface simulation based on Perlin noise and secondary distorted textures. In: Advances in Computer Science and Ubiquitous Computing: CSA-CUTE2016 8. Springer Singapore, pp. 236–245. https://doi.org/10.1007/978-981-10-3023-9_39.

Limerinos, J.T., 1970. Determination of the Manning Coefficient from Measured Bed Roughness in Natural Channels, vol. 1898. US Government Printing Office, Washington, DC.

Manning, R., (1891). On the flow of water in open channels and pipes. Ireland. Institute of Civil Engineers Trans. Pag. 161-207.

Maruffi, L., Stucchi, L., Casale, F., Bocchiola, D., 2022. Soil erosion and sediment transport under climate change for Mera River, in Italian Alps of Valchiavenna. Sci. Total Environ. 806, 150651 https://doi.org/10.1016/j.scitotenv.2021.150651.

Merwade, V., Cook, A., Coonrod, J., 2008. GIS techniques for creating river terrain models for hydrodynamic modeling and flood inundation mapping. Environ. Model. Software 23 (10–11), 1300–1311. https://doi.org/10.1016/j.envsoft.2008.03.005.

Michot-Roberto, S., Garcia-Hernández, A., Dopazo-Hilario, S. et al. The spherical primitive and perlin noise method to recreate realistic aggregate shapes. Granul. Matter 23, 41 (2021). doi:https://doi.org/10.1007/s10035-021-01105-6Langbein, W. B., & Leopold, L. B. (1964). Quasi-equilibrium states in channel morphology. *American Journal of Science*, *262*(6), 782–794. doi:https://doi.org/10.2475/ajs.262.6.782.

Milhous, R.T., Wegner, D.L., Waddle, T., 1984. User's Guide to the Physical Habitat Simulation System (PHABSIM) (no. 11). Department of the Interior, US Fish and Wildlife Service.

Nikora, V., Goring, D., McEwan, I., Griffiths, G., 2001. Spatially averaged open-channel flow over rough bed. J. Hydraul. Eng. 127 (2), 123–133. https://doi.org/10.1061/(ASCE)0733-9429(2001)127:2(123).

Perlin, K., 1985. An image synthesizer. ACM Siggraph Computer Graphics 19 (3), 287–296.

Richards, K.S., 1976. The morphology of riffle-pool sequences. Earth Surface Processes 1 (1), 71–88. https://doi.org/10.1002/esp.3290010108.

Richardson, L.F., 1922. Weather Prediction by Numerical Process. Cambridge Univ. Press, New York.

Roni, P., Hall, J.E., Drenner, S.M., Arterburn, D., 2019. Monitoring the effectiveness of floodplain habitat restoration: a review of methods and recommendations for future monitoring. Wiley Interdiscip. Rev. Water 6 (4), e1355. https://doi.org/10.1002/wat2.1355.

Salmaso, F., Servanzi, L., Crosa, G., Quadroni, S., Espa, P., 2021. Assessing the impacts of hydropeaking on river benthic macroinvertebrates: a state-of-the-art methodological overview. Environments 8 (7), 67. https://www.mdpi.com/2076-3298/8/7/67.

Servanzi, L., Quadoni, S., Espa, P., 2023. Hydro-morphological alteration and related effects on fish habitat induced by sediment management in a regulated alpine river. Int. J. Sediment Res. https://www.sciencedirect.com/science/article/pii/S1001627923000665.

Song, Y., Huang, J., Toorman, E., Yang, G., 2020. Reconstruction of river topography for 3d hydrodynamic modelling using surveyed cross-sections: an improved algorithm. Water 12 (12), 3539. https://doi.org/10.3390/w12123539.

Steffler, P., Ghanem, A., Blackburn, J., 2002. River2D Version 0.90, University of Alberta, Fisheries and Oceans, Canada, and United States Geological Survey.

Stucchi, L., Bignami, D.F., Bocchiola, D., Del Curto, D., Garzulino, A., Rosso, R., 2021. Assessment of climate-driven flood risk and adaptation supporting the conservation management plan of a heritage site. The national art schools of Cuba. Climate 9 (2), 23. https://doi.org/10.3390/cli9020023.

Tazioli, A., 2011. Experimental methods for river discharge measurements: comparison among tracers and current meter. Hydrol. Sci. J. 56 (7), 1314–1324. https://doi.org/10.1080/02626667.2011.607822.

Teng, J., Jakeman, A.J., Vaze, J., Croke, B.F., Dutta, D., Kim, S.J.E.M., 2017. Flood inundation modelling: a review of methods, recent advances and uncertainty analysis. Environ. Model. Software 90, 201–216.

Williams, R.D., Brasington, J., Hicks, D.M., 2016. Numerical modelling of braided river morphodynamics: review and future challenges. Geogr. Compass 10 (3), 102–127. https://doi.org/10.1111/gec3.12260.